

Recessive Osteogenesis Imperfecta Caused by Missense Mutations in *SPARC*

Roberto Mendoza-Londono,^{1,2} Somayyeh Fahiminiya,³ Jacek Majewski,³ Care4Rare Canada Consortium, Martine Tétreault,³ Javad Nadaf,³ Peter Kannu,^{1,2} Etienne Sochett,^{2,4} Andrew Howard,^{2,5} Jennifer Stimec,^{2,6} Lucie Dupuis,^{1,2} Paul Roschger,⁷ Klaus Klaushofer,⁷ Telma Palomo,⁸ Jean Ouellet,⁸ Hadil Al-Jallad,⁸ John S. Mort,⁸ Pierre Moffatt,⁸ Sergei Boudko,⁹ Hans-Peter Bächinger,⁹ and Frank Rauch^{8,*}

Secreted protein, acidic, cysteine-rich (*SPARC*) is a glycoprotein that binds to collagen type I and other proteins in the extracellular matrix. Using whole-exome sequencing to identify the molecular defect in two unrelated girls with severe bone fragility and a clinical diagnosis of osteogenesis imperfecta type IV, we identified two homozygous variants in *SPARC* (GenBank: NM_003118.3; c.497G>A [p.Arg166His] in individual 1; c.787G>A [p.Glu263Lys] in individual 2). Published modeling and site-directed mutagenesis studies had previously shown that the residues substituted by these mutations form an intramolecular salt bridge in *SPARC* and are essential for the binding of *SPARC* to collagen type I. The amount of *SPARC* secreted by skin fibroblasts was reduced in individual 1 but appeared normal in individual 2. The migration of collagen type I alpha chains produced by these fibroblasts was mildly delayed on SDS-PAGE gel, suggesting some overmodification of collagen during triple helical formation. Pulse-chase experiments showed that collagen type I secretion was mildly delayed in skin fibroblasts from both individuals. Analysis of an iliac bone sample from individual 2 showed that trabecular bone was hypermineralized on the material level. In conclusion, these observations show that homozygous mutations in *SPARC* can give rise to severe bone fragility in humans.

Osteogenesis imperfecta (OI) is a heritable bone fragility disorder that most often is caused by mutations in *COL1A1* (MIM: 120150) or *COL1A2* (MIM: 120160), the genes that code for collagen type I alpha 1 and alpha 2 chains.^{1,2} Extraskelatal findings related to connective tissue disturbances, such as tooth abnormalities (dentogenesis imperfecta) and blue or gray sclera are often associated with mutations in these genes. Over the past decade, defects in various other genes have been identified that lead to dominantly and recessively inherited forms of OI (*BMP1* [MIM: 112264], *CREB3L1*, *CRTAP* [MIM: 605497], *FKBP10* [MIM: 607063], *IFITM5* [MIM: 614757], *LEPRE1* [MIM: 610339], *P4HB* [MIM: 176790], *PLOD2* [MIM: 601865], *PLS3* [MIM: 300131], *PP1B* [MIM: 123841], *SEC24D* [MIM: 607186], *SERPINF1* [MIM: 172860], *SERPINH1* [MIM: 600943], *SP7* [MIM: 606633], *TMEM38B* [MIM: 611236], *WNT1* [MIM: 164820]). These genes play a role in the processing of collagen type I or in the control of osteoblast differentiation or function.

Despite these advances in genetic information, a small proportion of individuals that present with a phenotype of severe OI do not have mutations in any of the genes that are known to be associated with OI. Here we report on two unrelated girls who had a clinical diagnosis of OI type IV (MIM: 166220; an OI type with severe bone

fragility) and who were found to carry two different homozygous missense mutations in *SPARC*.

Individual 1 is a girl of North African origin who was born by spontaneous vaginal delivery after 37 weeks of uncomplicated gestation with a birth weight of 3,000 g. No skeletal abnormalities were noted at birth. Her parents were non-consanguineous but were from the same geographically restricted area. Both parents were healthy and did not have a history of fractures. At 24 hr after birth, the girl had a right-sided focal seizure, and an intra-ventricular hemorrhage was diagnosed. No neurosurgical interventions were performed and no further episodes of cerebral hemorrhage were noted.

At 15 months of age, individual 1 sustained her first fracture (right proximal femur) when she fell while trying to stand up. Radiographic evaluation at 19 months of age in addition revealed multiple vertebral compression fractures of the thoracic spine and kyphoscoliosis; a diagnosis of OI type IV was made. Serum biochemistry revealed normal results for calcium, inorganic phosphorus, alkaline phosphatase, creatinine, and 25-hydroxy-vitamin D. When she was 21 months old, she was diagnosed with expressive and comprehensive speech delay. At 23 months she had surgery on the left eye for strabismus. Treatment with intravenous pamidronate infusions was started at 30 months of age, but scoliosis continued to increase.

¹Department of Paediatrics, Division of Clinical and Metabolic Genetics, The Hospital for Sick Children and University of Toronto, Toronto, ON M5G 1X8, Canada; ²The Bone Health Centre, The Hospital for Sick Children, Toronto, ON M5G 1X8, Canada; ³Department of Human Genetics, McGill University and Génome Québec Innovation Centre, Montréal, QC H3A 1B1, Canada; ⁴Division of Endocrinology, Department of Paediatrics, The Hospital for Sick Children and University of Toronto, Toronto, ON M5G 1X8, Canada; ⁵Department of Orthopaedic Surgery, The Hospital for Sick Children and The University of Toronto, Toronto, ON M5G 1X8, Canada; ⁶Department of Diagnostic Imaging, The Hospital for Sick Children, Toronto, ON M5G 1X8, Canada; ⁷Ludwig Boltzmann Institute of Osteology at the Hanusch Hospital of WGKK and AUVA Trauma Center Meidling, 1st Med. Department, Hanusch Hospital, Vienna 1140, Austria; ⁸Shriners Hospital for Children, Montréal, QC H3G 1A6, Canada; ⁹Shriners Hospital for Children, Portland, OR 97239, USA

*Correspondence: frauch@shriners.mcgill.ca

<http://dx.doi.org/10.1016/j.ajhg.2015.04.021>. ©2015 by The American Society of Human Genetics. All rights reserved.

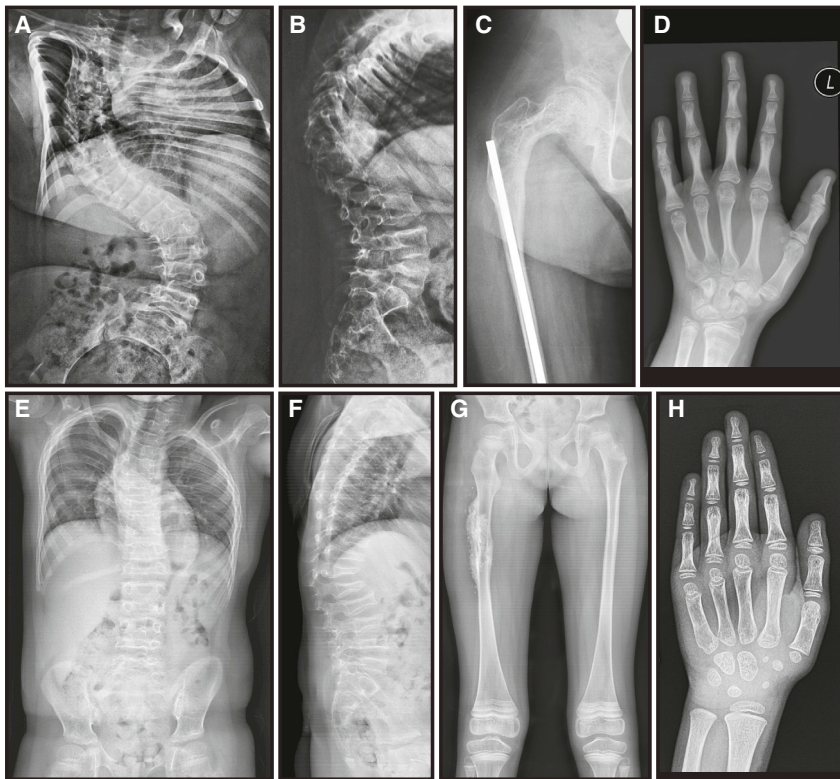


Figure 1. Phenotypic Findings in Individuals 1 and 2

(A and B) Anteroposterior and lateral views of the spine of individual 1 (age: 6 years), demonstrating severe scoliosis, kyphosis, and vertebral compression fractures.

(C) Right hip and proximal femur of individual 1 (age: 14 years). The femoral neck has a very small diameter. An intramedullary rod has been inserted to treat repeated fractures and femoral bowing.

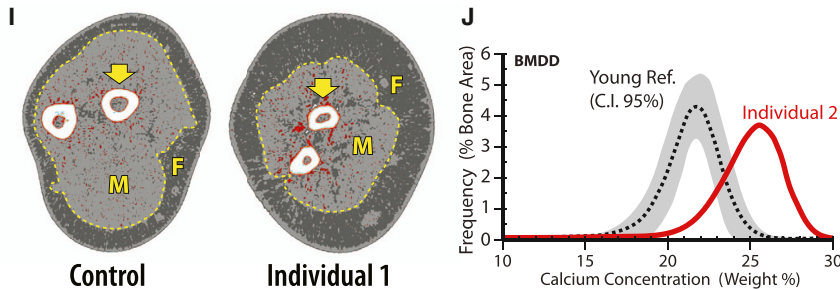
(D) Hand and wrist radiograph of individual 1 (age: 14 years), showing metaphyseal lines from prior intravenous pamidronate infusions. The skeletal maturation (bone age) corresponds to chronological age.

(E and F) Anteroposterior and lateral views of the spine of individual 2 (age: 6 years), showing mild scoliosis, kyphosis, and severe vertebral compression fractures.

(G) The femurs of individual 2 (age: 6 years) have a small diameter and thin cortices, but are straight. A callus is visible on the right femur after a diaphyseal fracture. Metaphyseal lines resulting from pamidronate infusions are also visible.

(H) Hand and wrist radiograph of individual 2 (age: 5 years), showing thin cortices of metacarpal bones but no dysplastic features.

(I) Forearm peripheral quantitative computed tomography of individual 1 at the age of 14 years, compared to a healthy control of the same age and sex. The size of the two forearm cross-sections is similar, but the outer size of the radius (marked by arrows) is much lower in individual 1 (total cross-sectional area of the radius: 57 mm²; age- and sex-matched Z score: -3.9) than in the control individual



(118 mm², Z score +0.9). The percentage of fat (dark gray area, marked by an F) in the forearm cross-section is increased (48%), compared to the control (28%). The reverse is true for muscle (light gray area, marked by an M).

(J) Bone mineralization density distribution in cancellous bone of individual 2. The curve labeled in gray represents pediatric reference data (mean and 95% confidence interval), as established previously in our laboratory.³⁷

By the time individual 1 was first assessed at our institution at the age of 4.4 years, she had sustained a total of ten long-bone fractures (seven femur fractures, three humerus fractures). Height (95 cm; Z score -1.9) and weight (14.5 kg; Z score -1.1) were in the lower part of the reference range. Sclerae were white and there was no dentinogenesis imperfecta but there was mild joint hyperlaxity (Table S1). Muscles of the lower extremities appeared underdeveloped and weak. Both humeri were bowed. The lumbar spine areal bone mineral density Z score (after almost 2 years of pamidronate treatment) was -3.1.

Intramedullary rodding procedures of both femurs were performed at 5.5 years of age (Figure 1C). Progressive scoliosis (Figures 1A and 1B) necessitated spinal fusion surgery at the age of 6.7 years. Despite these interventions, individual 1 has never achieved independent walking and she has sustained about one long-bone fracture per year. At the

time of the last follow up at 14 years of age, she was using a wheelchair for all mobility, height was 127 cm (Z score -5.2), and weight was 41.5 kg (Z score -1.8). Forearm peripheral quantitative computed tomography revealed a small cross-sectional bone size (Figure 1I), in accordance with the observation that diaphyses appeared slender on radiographs (Figures 1C and 1D). The serum level of pigment-epithelium derived factor was within normal limits (15.4 mg/l; range observed in healthy controls: 2.0 to 17.5 mg/l),³ excluding a diagnosis of OI type VI (MIM: 613982).

The mother of individual 1 (age: 41 years) had a lumbar spine areal bone mineral density Z score of +0.8. In the father (age: 60 years), the lumbar spine areal bone mineral density Z score was -1.0. Both parents also had normal results for peripheral quantitative computed tomography at the forearm (data not shown).

Individual 2 was born prematurely at 34 weeks gestation after premature rupture of membranes. Her birth weight was 2.0 kg, birth length 45 cm, and head circumference 32 cm (all within normal limits for gestational age). She was the older of two children of a consanguineous couple of Indian descent. Family history was negative for muscle and bone fragility disorders.

Left hip dislocation was noted at the age of 10 weeks and was treated with serial casting until 9 months of age. Her cognitive, language, and hearing development were normal, but she had muscle hypotonia and gross motor developmental delay (Table S1). She started rolling over at 10 months, crawling at 18 months, and walking independently at 3 years of age. Joint hyperlaxity was noted. Concentrations of plasma amino acids, serum creatine kinase, creatine, acylcarnitine profile, ammonia, lactate, and urine organic acids were normal. Sequencing of *COL6A1*, *COL6A2*, *COL6A3*, and *SEPN1* was done due to muscle hypotonia and did not reveal any abnormalities. Microarray analysis for copy number variations using a 180K oligonucleotide array was normal.

On physical examination at 5 years of age, her weight was 14.4 kg (*Z* score -1.2), height 102 cm (*Z* score -1.0), and head circumference 51 cm (*Z* score 0.0). Lower extremity weakness and decreased muscle mass in the calf muscles were noted. MRI of the brain and spine at 4 years of age showed non-specific abnormal fluid-attenuated inversion recovery signal in the para-atrial white matter, a large spinal canal with syrinx from T10 to L1, generalized platyspondyly, and thoracic kyphosis. There was joint hyperlaxity and soft skin without signs of exaggerated scarring. Teeth appeared normal on inspection.

Individual 2 was 7 years old at her last evaluation. She sustained her first low-trauma fracture at 5 years of age (mid-shaft transverse femur fracture after a low-impact fall) and has had five fractures since then (bilateral distal radius with no identifiable cause, transverse bilateral fractures of the pubic ramus, and mid-diaphyseal of left femur). At 6 years of age, skeletal radiographs showed compression fractures of most thoracic and lumbar vertebra, and mild kyphoscoliosis (Figures 1E and 1F). Long bones were straight (Figure 1G). Bone age corresponded to chronological age (Figure 1H). Dual-energy X-ray absorptiometry revealed a lumbar spine areal bone mineral density *Z* score of -4.0 . An iliac bone sample was obtained, which due to severe fragility was not sufficiently preserved for quantitative histomorphometric evaluation, but showed normal tetracycline uptake, indicating the absence of a mineralization disorder such as osteomalacia (Figure S1). Bone mineralization density distribution of mineralized trabecular bone as measured by quantitative backscattered electron imaging in the same sample was shifted to higher values, suggesting hypermineralization on the material level (Figure 1J).⁴ Given the fracture history and low bone mineral density by dual-energy X-ray absorptiometry, treatment with intravenous pamidronate was started at 6 years of age.

To identify the disease-causing genetic defect in these two girls, we performed whole-exome sequencing on genomic DNA after obtaining approval from the Institutional Review Board of McGill University and the Hospital for Sick Children and informed consent from the two families. Agilent SureSelect Human All Exon Kit version 4 (individual 1) and 5 (individual 2) were used for target enrichment, and 100 base pair paired-end runs on an Illumina HiSeq 2000 device at Genome Quebec and McGill University Innovation Center as previously detailed.⁵ The bioinformatics analysis of exome sequencing data was carried out as described previously.^{6,7} In brief, we used BWA (v.0.5.9) for mapping of reads against the human reference genome (hg19), Samtools mpileup (v.0.1.17) for variant calling, and ANNOVAR⁸ for variants annotation. A mean coverage of 135 \times (individual 1) and 115 \times (individual 2) was obtained for all consensus coding sequence exons and 97% of bases were covered by ≥ 5 reads as determined by the Genome Analysis Toolkit.

The analysis of sequencing results focused on exonic and canonical splice site variants with possible protein altering effects (nonsense, frameshift indel, splicing, and missense). Only variants covered by at least 5 reads and a quality score higher than 20 were considered. We filtered out the variants that had an allele frequency $>5\%$ in either the 1000 Genomes database or the NHLBI/NHGRI Exome Project (v.0.0.14, June 20, 2012) or were seen in >30 individuals in our exome database (more than 1,000 exomes) or that occurred as homozygotes in the ExAC database. This resulted in 485 and 327 variants in individual 1 and 2, respectively. None of the observed variants occurred in genes that were known to be associated with dominant or recessive OI. In both individuals, compound heterozygous variants were found in several genes that have not been linked to bone fragility (Table S2). In each of these genes, only one or neither of the variants were predicted to be damaging by three different bioinformatics algorithms (SIFT,⁹ PolyPhen-2,¹⁰ MutationTaster¹¹).

The family histories suggested recessive inheritance, so we focused on homozygous variants (Table S2). The only gene in which both individual 1 and individual 2 had homozygous variants was *SPARC* (MIM: 1821200; GenBank: NM_003118.3; Figure S2). In both individuals *SPARC* was part of a region of homozygosity, which was 18.5 Mb in size for individual 1 and 22 Mb for individual 2 (Figure S3). Even though consanguinity was known from medical history only for the parents of individual 2, these data indicate that the parents of individual 1 also shared common ancestry. In individual 1 we identified a nonsynonymous homozygous variant (c.497G>A [p.Arg166His]) in exon 7. In individual 2, we observed a homozygous missense variant (c.787G>A [p.Glu263Lys]) in exon 9. Neither variant were present in the databases of dbSNP, 1000 Genomes, the NHLBI/NHGRI Exome Project, or ExAC and were not previously seen in our in-house exome database. Moreover, both variants were predicted to be damaging by the three bioinformatics algorithms.

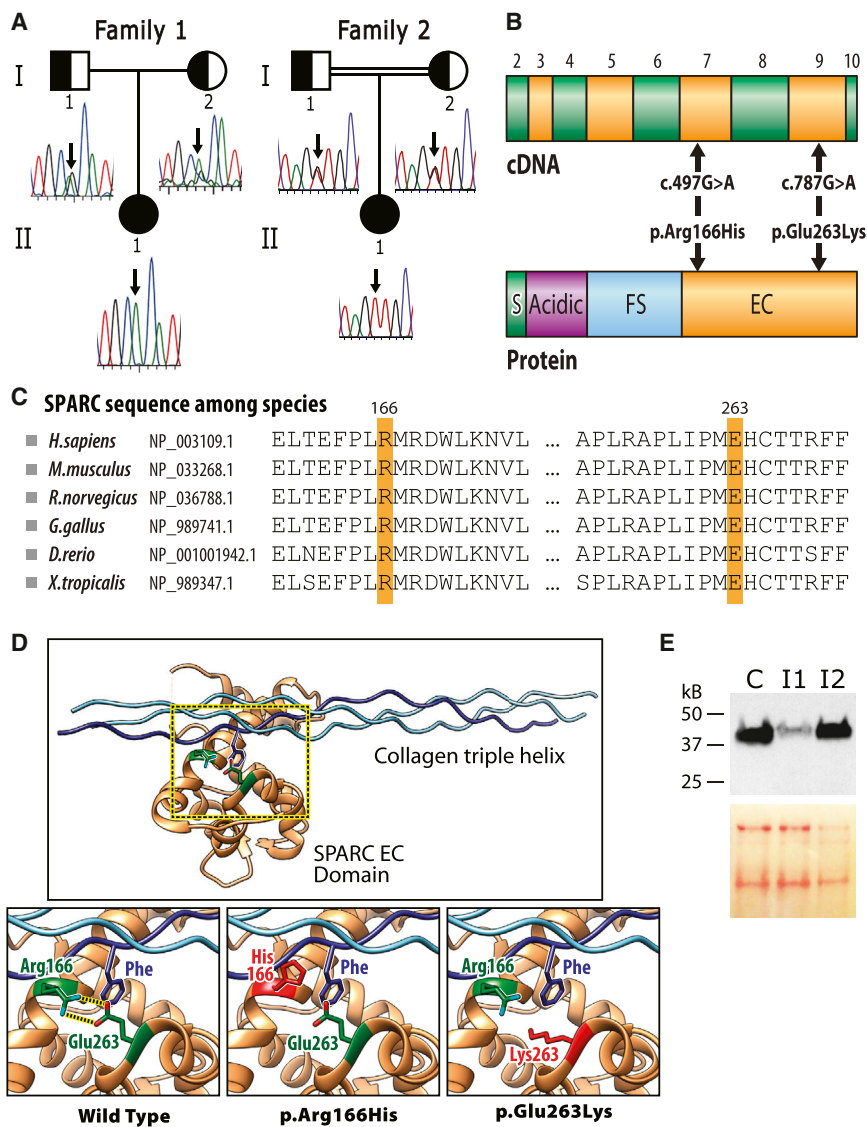


Figure 2. Confirmation of the Homozygous SPARC Mutations and Prediction of Their Impact on SPARC

(A) Sanger sequencing results of individuals 1 and 2 and their parents. Individual 1 (II-1 in family 1) is homozygous for the c.497G>A variant, and both parents are heterozygous. Individual 2 (II-1 in family 2) is homozygous for the c.787G>A variant, and both parents are heterozygous.

(B) Schematic representation of the coding exons of SPARC cDNA (GenBank: NM_003118.3) and of SPARC protein (GenBank: NP_003109.1). The locations of the exons are aligned relative to the regions of the SPARC protein that each exon encodes. The positions of the mutations reported in the present study are indicated. Abbreviations are as follows: S, signal peptide; Acidic, acidic domain; FS, follistatin-like domain; EC, extracellular collagen binding domain.

(C) The mutated SPARC residues Arg166 and Glu263 and several adjoining residues at each site are perfectly conserved among species.

(D) Modeling of the interaction between SPARC and collagen type I. Top: SPARC EC domain with the triple helical collagen type I alpha chains shown in light blue (alpha 1 chain) and dark blue (alpha 2 chain). Bottom: the critical regions of SPARC and collagen type I are magnified. The Phe residue of the alpha 1 chain is surrounded by the “Phe pocket” of SPARC.¹³ Arg166 and Glu263 form a salt bridge that is critical for maintaining the Phe pocket. When Arg166 or Glu263 are substituted by other residues, the loop conformation of the Phe pocket can not be maintained and collagen binding is impaired.²⁶

(E) Immunoblot of SPARC protein in conditioned medium of skin fibroblasts

from a control individual (C) and from individuals 1 (I1) and 2 (I2). The amount of SPARC in the medium is clearly lower in individual 1. Ponceau staining (bottom) shows equal loading in the control and individual 1, but somewhat lower loading for individual 2.

Sanger sequencing confirmed that both individuals were homozygous for these mutations (Figure 2A). Parents were heterozygous for the respective mutation.

SPARC is expressed mainly in cells with high rates of extracellular matrix production¹² and it codes for secreted protein, acidic, cysteine-rich (SPARC), which has also been called osteonectin and BM-40. SPARC binds to collagen type I and other matrix proteins.^{13–15} It is counted among the matricellular proteins, a group of non-structural extracellular proteins that modulate cell-matrix interaction.¹⁶

In bone, SPARC is expressed by osteoblasts. SPARC-null mice develop progressive osteoporosis, due to a defect in bone formation.¹⁷ These mice also develop other abnormalities, such as intervertebral disc degeneration and decreased muscle mass.^{18–20} A polymorphism in the SPARC 3' UTR influences SPARC accumulation in bone, is associated with variations in bone formation and bone mass,

and might play a role in the pathogenesis of osteoporosis in adults.^{21,22} SPARC synthesis is low in primary osteoblasts from children with OI and SPARC content is low in OI bone.²³ SPARC has also been implicated in a number of common disorders, such as insulin resistance, fibrosing disorders, and several types of cancer.^{15,24,25}

SPARC residues Arg166 and Glu263 are strictly conserved in evolution and are located in the EC domain of the protein (Figures 2B and 2C). Even though spaced far apart in the linear amino acid sequence, Arg166 and Glu263 directly interact with each other in the three-dimensional structure of the SPARC protein (Figure 2D).¹³ Arg166 and Glu263 form an intramolecular salt bridge that is essential for maintaining the structure (“Phe pocket”) through which SPARC binds to fibrillar collagens. The importance of SPARC residues Arg166 and Glu263 for collagen type I binding has previously been demonstrated by detailed site-directed

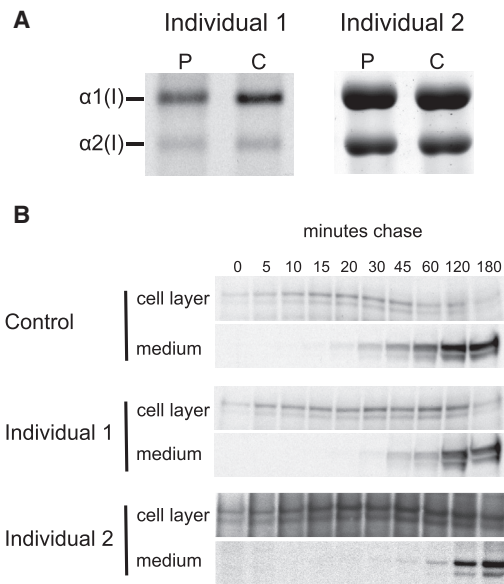


Figure 3. Collagen Type I Studies in Skin Fibroblasts

(A) Biochemical analysis of collagen type I in the cell layer. Skin fibroblasts of individuals 1 and 2 (P) synthesize collagen type I alpha chains that have a very mild delay in migration, as compared to a control sample (C).

(B) Pulse-chase analysis of collagen type I secretion. The bands in each set represent the collagen trimers that migrated into the gel under nonreducing conditions. In individuals 1 and 2, there is a delay in secretion of the type I collagen trimer.

mutagenesis studies, which showed that substituting either of these residues abolishes the affinity of SPARC to collagen type I.²⁶

We assessed the effects of the SPARC variants in skin fibroblasts from individuals 1 and 2. The amount of SPARC secreted by these cells was reduced in individual 1 but appeared normal in individual 2 (Figure 2E).

Even though SPARC is a secreted protein and binds to collagen type I in the extracellular space, it might also play a role as an intracellular chaperone of collagen type I.²⁷ We therefore evaluated collagen type I production in fibroblasts. Delays in collagen type I triple helical formation typically lead to overmodification of collagen alpha chains.²⁸ SDS-PAGE showed a mild delay in the migration of collagen type I alpha chains, suggesting some overmodification of the alpha chains (Figure 3A). Pulse-chase experiments indicated a delay in the secretion of procollagen type I (Figure 3B).

Here we report on two girls with severe bone fragility due to homozygous missense mutations in *SPARC*. The mutations affected two residues that had previously been shown to directly interact with each other, forming an intramolecular salt bridge that is essential for SPARC binding to collagen type I.²⁶ Given the role of SPARC in collagen type I fiber assembly and the osteopenic phenotype of the *SPARC*-deficient mouse,^{17,29} it is not unexpected that homozygous mutations in *SPARC* can lead to bone fragility in humans. Apart from severe bone fragility, individual 1 had severe early-onset scoliosis. A role of SPARC in the

spine is suggested also in the *Sparc*-null mouse, which develops disc degeneration.¹⁹

In addition to the skeletal disease manifestations, individual 1 also was diagnosed with intraventricular hemorrhage in the immediate postnatal period. SPARC is dynamically produced in blood vessels during central nervous system development.³⁰ It is thus possible that the intraventricular hemorrhage observed in the immediate postnatal period was related to the defect in SPARC, even though a causal link is difficult to prove.

The clinical phenotype of the two girls with *SPARC* mutations has some similarities with that of OI type VI, which is caused by loss of function in *SERPINF1*. In both situations, children do not have obvious skeletal abnormalities at birth but then develop severe bone fragility. It also appears from our backscattered electron imaging data that *SPARC* mutations can be associated with bone hypermineralization on the material level, which is similar to OI caused by *SERPINF1* mutations.³⁰ However, the bone histological hallmark of OI type VI, blurred tetracycline label indicating a mineralization defect, was not present in the bone sample of individual 2, and in contrast to what is observed in OI type VI, the serum concentration of pigment-epithelium derived factor was normal in individual 1.³ Thus, despite the clinical similarities, OI caused by *SPARC* mutations is clearly distinct from OI type VI.

The heterozygous parents of the two individuals did not have a history of fractures. The bone density tests of the parents of individual 1 yielded normal results. This is in accordance with the observation that the heterozygous *Sparc* knockout mouse also does not have a bone phenotype.¹⁷ Similarly, carriers of mutations in *CRTAP*, *LEPRE1*, and other mutations coding for collagen-modifying proteins typically have normal bone mass.^{31,32} In contrast, heterozygous carriers of mutations in WNT signaling pathway genes such as *LRP5* and *WNT1* tend to have low bone mass^{33–35} but no hypermineralization.^{5,36}

In conclusion, this report identifies recessive mutations in *SPARC* as a cause of severe OI.

Supplemental Data

Supplemental Data include three figures and two tables and can be found with this article online at <http://dx.doi.org/10.1016/j.ajhg.2015.04.021>.

Acknowledgments

We thank Patty Mason for technical assistance and Mark Lepik for the preparation of the figures. F.R. received support from the Chercheur-Boursier Clinicien program of the Fonds de Recherche du Québec - Santé. J.M. is a recipient of a Canada Research Chair. We also wish to acknowledge the contribution of the high-throughput and Sanger sequencing platforms of the McGill University and Genome Québec Innovation Centre (Montreal, Canada). Quantitative backscattered electron imaging was performed at the Bone Material Laboratory of the Ludwig Boltzmann Institute of Osteology, Vienna, Austria. We thank D. Gabriel,

P. Keplinger, S. Lueger, and P. Messmer for technical assistance with sample preparation and backscattered electron imaging measurements. This work was supported by the AUVA (Austrian Social Insurance for Occupational Risk) and the WGKK (Social Health Insurance Vienna). This study was also supported by the Shriners of North America. This disorder was selected for study by the Care4Rare Canada (Enhanced Care for Rare Genetic Diseases in Canada) Consortium Gene Discovery Steering Committee: Kym Boycott (lead; University of Ottawa), Alex MacKenzie (co-lead; University of Ottawa), J.M. (McGill University), Michael Brudno (University of Toronto), Dennis Bulman (University of Ottawa), and David Dymant (University of Ottawa). It was funded, in part, by Genome Canada, the Canadian Institutes of Health Research, the Ontario Genomics Institute, Ontario Research Fund, Genome Quebec, Children's Hospital of Eastern Ontario Foundation, and the Hospital for Sick Children.

Received: February 27, 2015

Accepted: April 28, 2015

Published: May 28, 2015

Web Resources

The URLs for data presented herein are as follows:

1000 Genomes, <http://browser.1000genomes.org>
 dbSNP, <http://www.ncbi.nlm.nih.gov/projects/SNP/>
 ExAC Browser, <http://exac.broadinstitute.org/>
 Exome Project, <http://exome.gs.washington.edu/>
 Human Gene Mutation Database, <http://www.hgmd.org/>
 OMIM, <http://www.omim.org/>
 RCSB Protein Data Bank, <http://www.rcsb.org/pdb/home/home.do>
 RefSeq, <http://www.ncbi.nlm.nih.gov/RefSeq>
 UCSC Genome Browser, <http://genome.ucsc.edu>

References

- Forlino, A., Cabral, W.A., Barnes, A.M., and Marini, J.C. (2011). New perspectives on osteogenesis imperfecta. *Nat. Rev. Endocrinol.* *7*, 540–557.
- Marini, J.C., and Blissett, A.R. (2013). New genes in bone development: what's new in osteogenesis imperfecta. *J. Clin. Endocrinol. Metab.* *98*, 3095–3103.
- Rauch, F., Hussein, A., Roughley, P., Glorieux, F.H., and Mofatt, P. (2012). Lack of circulating pigment epithelium-derived factor is a marker of osteogenesis imperfecta type VI. *J. Clin. Endocrinol. Metab.* *97*, E1550–E1556.
- Roschger, P., Paschalis, E.P., Fratzl, P., and Klaushofer, K. (2008). Bone mineralization density distribution in health and disease. *Bone* *42*, 456–466.
- Fahiminiya, S., Majewski, J., Roughley, P., Roschger, P., Klaushofer, K., and Rauch, F. (2013). Whole-exome sequencing reveals a heterozygous LRP5 mutation in a 6-year-old boy with vertebral compression fractures and low trabecular bone density. *Bone* *57*, 41–46.
- Fahiminiya, S., Majewski, J., Mort, J., Mofatt, P., Glorieux, F.H., and Rauch, F. (2013). Mutations in WNT1 are a cause of osteogenesis imperfecta. *J. Med. Genet.* *50*, 345–348.
- McDonald-McGinn, D.M., Fahiminiya, S., Revil, T., Nowakowska, B.A., Suhl, J., Bailey, A., Mlynarski, E., Lynch, D.R., Yan, A.C., Bilaniuk, L.T., et al. (2013). Hemizygous mutations in SNAP29 unmask autosomal recessive conditions and contribute to atypical findings in patients with 22q11.2DS. *J. Med. Genet.* *50*, 80–90.
- Wang, K., Li, M., and Hakonarson, H. (2010). ANNOVAR: functional annotation of genetic variants from high-throughput sequencing data. *Nucleic Acids Res.* *38*, e164.
- Kumar, P., Henikoff, S., and Ng, P.C. (2009). Predicting the effects of coding non-synonymous variants on protein function using the SIFT algorithm. *Nat. Protoc.* *4*, 1073–1081.
- Adzhubei, I.A., Schmidt, S., Peshkin, L., Ramensky, V.E., Gerasimova, A., Bork, P., Kondrashov, A.S., and Sunyaev, S.R. (2010). A method and server for predicting damaging missense mutations. *Nat. Methods* *7*, 248–249.
- Schwarz, J.M., Rödelberger, C., Schuelke, M., and Seelow, D. (2010). MutationTaster evaluates disease-causing potential of sequence alterations. *Nat. Methods* *7*, 575–576.
- Mundlos, S., Schwahn, B., Reichert, T., and Zabel, B. (1992). Distribution of osteonectin mRNA and protein during human embryonic and fetal development. *J. Histochem. Cytochem.* *40*, 283–291.
- Hohenester, E., Sasaki, T., Giudici, C., Farndale, R.W., and Bächinger, H.P. (2008). Structural basis of sequence-specific collagen recognition by SPARC. *Proc. Natl. Acad. Sci. USA* *105*, 18273–18277.
- Bradshaw, A.D. (2012). Diverse biological functions of the SPARC family of proteins. *Int. J. Biochem. Cell Biol.* *44*, 480–488.
- Kos, K., and Wilding, J.P. (2010). SPARC: a key player in the pathologies associated with obesity and diabetes. *Nat. Rev. Endocrinol.* *6*, 225–235.
- Murphy-Ullrich, J.E., and Sage, E.H. (2014). Revisiting the matricellular concept. *Matrix Biol.* *37*, 1–14.
- Delany, A.M., Amling, M., Priemel, M., Howe, C., Baron, R., and Canalis, E. (2000). Osteopenia and decreased bone formation in osteonectin-deficient mice. *J. Clin. Invest.* *105*, 915–923.
- Gilmour, D.T., Lyon, G.J., Carlton, M.B., Sanes, J.R., Cunningham, J.M., Anderson, J.R., Hogan, B.L., Evans, M.J., and Colledge, W.H. (1998). Mice deficient for the secreted glycoprotein SPARC/osteonectin/BM40 develop normally but show severe age-onset cataract formation and disruption of the lens. *EMBO J.* *17*, 1860–1870.
- Gruber, H.E., Sage, E.H., Norton, H.J., Funk, S., Ingram, J., and Hanley, E.N., Jr. (2005). Targeted deletion of the SPARC gene accelerates disc degeneration in the aging mouse. *J. Histochem. Cytochem.* *53*, 1131–1138.
- Bradshaw, A.D., Graves, D.C., Motamed, K., and Sage, E.H. (2003). SPARC-null mice exhibit increased adiposity without significant differences in overall body weight. *Proc. Natl. Acad. Sci. USA* *100*, 6045–6050.
- Delany, A.M., McMahon, D.J., Powell, J.S., Greenberg, D.A., and Kurland, E.S. (2008). Osteonectin/SPARC polymorphisms in Caucasian men with idiopathic osteoporosis. *Osteoporos. Int.* *19*, 969–978.
- Dole, N.S., Kapinas, K., Kessler, C.B., Yee, S.P., Adams, D.J., Pereira, R.C., and Delany, A.M. (2015). A single nucleotide polymorphism in osteonectin 3' untranslated region regulates bone volume and is targeted by miR-433. *J. Bone Miner. Res.* *30*, 723–732.
- Fisher, L.W., Drum, M.A., Robey, P.G., Conn, K.M., and Termine, J.D. (1987). Osteonectin content in human osteogenesis

- imperfecta bone shows a range similar to that of two bovine models of OI. *Calcif. Tissue Int.* *40*, 260–264.
24. Trombetta-Esilda, J., and Bradshaw, A.D. (2012). The function of SPARC as a mediator of fibrosis. *Open Rheumatol. J.* *6*, 146–155.
 25. Nagaraju, G.P., Dontula, R., El-Rayes, B.F., and Lakka, S.S. (2014). Molecular mechanisms underlying the divergent roles of SPARC in human carcinogenesis. *Carcinogenesis* *35*, 967–973.
 26. Sasaki, T., Hohenester, E., Göhring, W., and Timpl, R. (1998). Crystal structure and mapping by site-directed mutagenesis of the collagen-binding epitope of an activated form of BM-40/SPARC/osteonectin. *EMBO J.* *17*, 1625–1634.
 27. Martinek, N., Shahab, J., Sodek, J., and Ringuette, M. (2007). Is SPARC an evolutionarily conserved collagen chaperone? *J. Dent. Res.* *86*, 296–305.
 28. Ishikawa, Y., and Bächinger, H.P. (2013). A molecular ensemble in the rER for procollagen maturation. *Biochim. Biophys. Acta* *1833*, 2479–2491.
 29. Rentz, T.J., Poobalarahi, F., Bornstein, P., Sage, E.H., and Bradshaw, A.D. (2007). SPARC regulates processing of procollagen I and collagen fibrillogenesis in dermal fibroblasts. *J. Biol. Chem.* *282*, 22062–22071.
 30. Vincent, A.J., Lau, P.W., and Roskams, A.J. (2008). SPARC is expressed by macroglia and microglia in the developing and mature nervous system. *Dev. Dyn.* *237*, 1449–1462.
 31. Morello, R., Bertin, T.K., Chen, Y., Hicks, J., Tonachini, L., Monticone, M., Castagnola, P., Rauch, F., Glorieux, F.H., Vranka, J., et al. (2006). CRTAP is required for prolyl 3-hydroxylation and mutations cause recessive osteogenesis imperfecta. *Cell* *127*, 291–304.
 32. Cabral, W.A., Chang, W., Barnes, A.M., Weis, M., Scott, M.A., Leikin, S., Makareeva, E., Kuznetsova, N.V., Rosenbaum, K.N., Tiffit, C.J., et al. (2007). Prolyl 3-hydroxylase 1 deficiency causes a recessive metabolic bone disorder resembling lethal/severe osteogenesis imperfecta. *Nat. Genet.* *39*, 359–365.
 33. Gong, Y., Slee, R.B., Fukai, N., Rawadi, G., Roman-Roman, S., Reginato, A.M., Wang, H., Cundy, T., Glorieux, F.H., Lev, D., et al.; Osteoporosis-Pseudoglioma Syndrome Collaborative Group (2001). LDL receptor-related protein 5 (LRP5) affects bone accrual and eye development. *Cell* *107*, 513–523.
 34. Keupp, K., Beleggia, F., Kayserili, H., Barnes, A.M., Steiner, M., Semler, O., Fischer, B., Yigit, G., Janda, C.Y., Becker, J., et al. (2013). Mutations in WNT1 cause different forms of bone fragility. *Am. J. Hum. Genet.* *92*, 565–574.
 35. Laine, C.M., Joeng, K.S., Campeau, P.M., Kiviranta, R., Tarkkainen, K., Grover, M., Lu, J.T., Pekkinen, M., Wessman, M., Heino, T.J., et al. (2013). WNT1 mutations in early-onset osteoporosis and osteogenesis imperfecta. *N. Engl. J. Med.* *368*, 1809–1816.
 36. Palomo, T., Al-Jallad, H., Moffatt, P., Glorieux, F.H., Lentle, B., Roschger, P., Klaushofer, K., and Rauch, F. (2014). Skeletal characteristics associated with homozygous and heterozygous WNT1 mutations. *Bone* *67*, 63–70.
 37. Fratzl-Zelman, N., Roschger, P., Misof, B.M., Pfeffer, S., Glorieux, F.H., Klaushofer, K., and Rauch, F. (2009). Normative data on mineralization density distribution in iliac bone biopsies of children, adolescents and young adults. *Bone* *44*, 1043–1048.

The American Journal of Human Genetics

Supplemental Data

Recessive Osteogenesis Imperfecta

Caused by Missense Mutations in *SPARC*

Roberto Mendoza-Londono, Somayyeh Fahiminiya, Jacek Majewski, Care4Rare Canada Consortium, Martine Tétreault, Javad Nadaf, Peter Kannu, Etienne Sochett, Andrew Howard, Jennifer Stimec, Lucie Dupuis, Paul Roschger, Klaus Klaushofer, Telma Palomo, Jean Ouellet, Hadil Al-Jallad, John S. Mort, Pierre Moffatt, Sergei Boudko, Hans-Peter Bächinger, and Frank Rauch

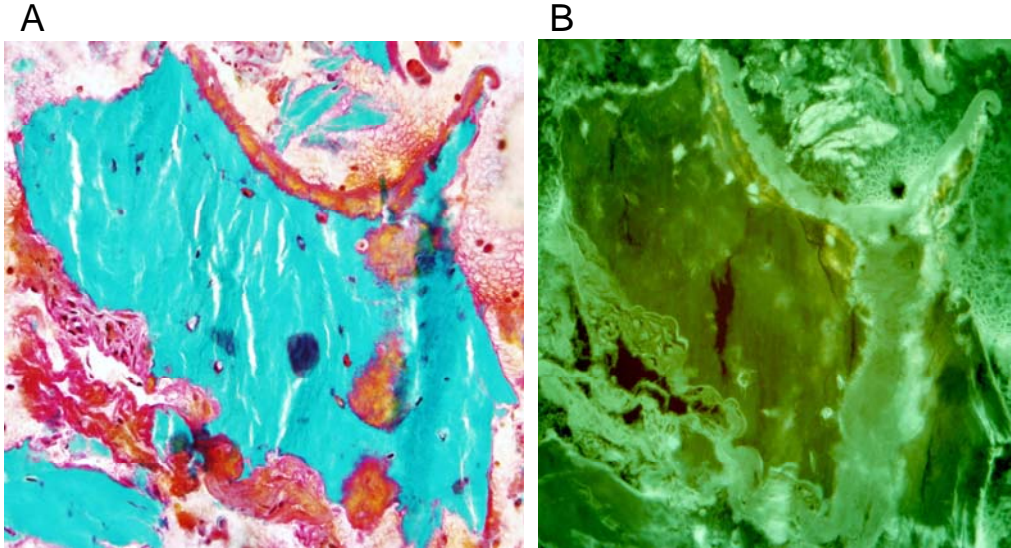


Figure S1. Iliac Bone Sample from Individual 2. Consecutive Sections of a Trabecula.

A. Goldner staining. Both the mineralized bone (in green) and the unmineralized osteoid (orange) have a normal aspect. B. Under fluorescent light, two tetracycline labels can be clearly distinguished (yellow bands), indicating that there is no mineralization disorder.

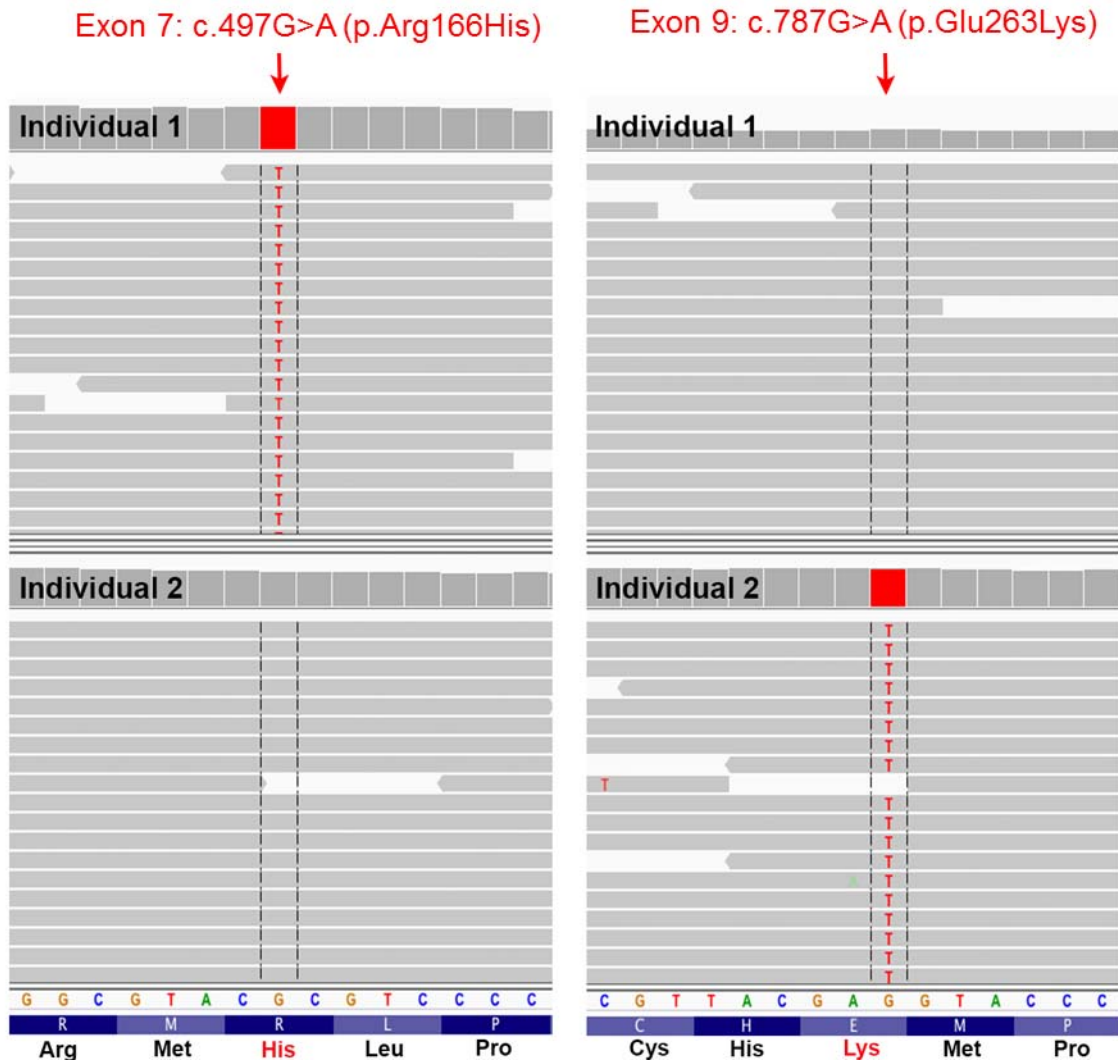


Figure S2. Identification of Homozygous Variants in SPARC in Individuals 1 and 2.

Visualization of the the 100 bp paired-end reads aligned to the positive strand of human genome (hg19) in IGV. Note that *SPARC* is transcribed from the negative strand. The annotation of the mutation marked by the red arrow therefore is c.497G>A and c.787G>A, which correspond to genomic positions of chr5:151047116 (individual 1) and chr5:151043744 (individual 2), respectively. The *SPARC* nucleotide (NM_003118.3) and corresponding amino acid sequences are shown in the lower panel. The Integrative Genomics Viewer (IGV) was used to visualize the identified variants.

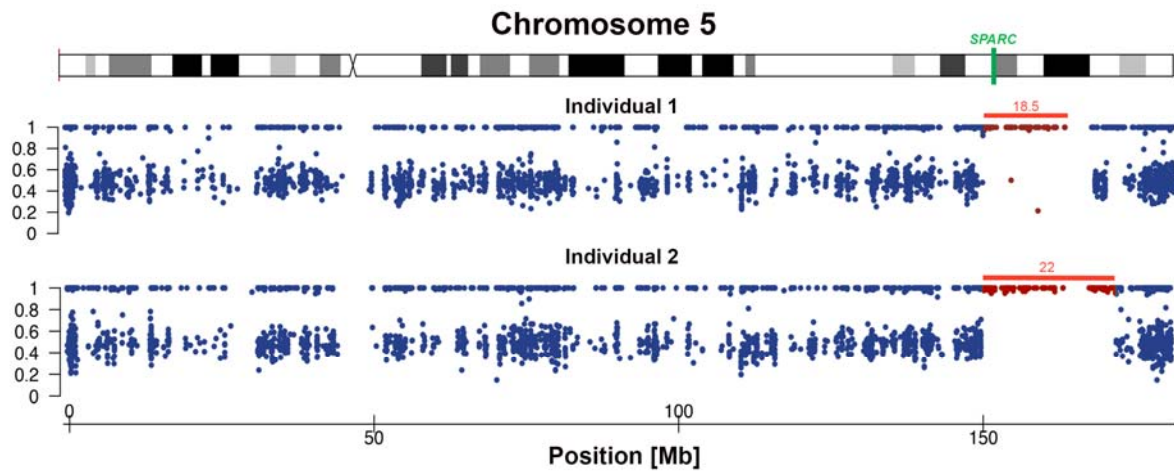


Figure S3. Plot of B Allele Frequency on Chromosome 5.

Each blue dot represents a variant identified by whole-exome sequencing. The x-axis shows positions of the variants on chromosome 5 and the y-axis shows the B allele frequency. For each position, values around 0.5 correspond to heterozygous variants; a value of 1 indicates homozygosity for the B allele. The ~18.5 MB (Individual 1) and ~22 MB (Individual 2) regions of homozygosity surrounding *SPARC* are indicated by red dots and a red bar. The location of *SPARC* on chromosome 5 is indicated by a green vertical line.

Table S1. Clinical characteristics of two Individuals with SPARC mutations.

	Individual 1	Individual 2
Wormian bones	No	Not known
Cognitive function	Speech delay	Normal cognitive function Severe motor delay
Sclera	White	Slightly grey
Teeth	Normal	Normal
Hearing	Normal	Normal
Vision	Strabismus	Normal
Age at first fracture (months)	15	60
Height (z-score)	-5.4 (age 14 years)	-0.8 (age 6.8 years)
Lumbar spine areal BMD before pamidronate treatment (z-score)	Not available	-4.0 (age 6 years)
Long-bone deformities	Yes	No
Scoliosis	Yes	Mild
Vertebral compression fractures	Yes	Yes
Mobility	Wheelchair	Assisted ambulation
Serum biochemistry (calcium, inorganic phosphorus, alkaline phosphatase, parathyroid hormone)	Normal	Normal

BMD, bone mineral density

Table S2: Variant filtering strategy and identification of SPARC mutations

Variant filtering step	Individual 1	Individual 2
Total variants (N)	192286	202081
Nonsense/frameshift, Indel/canonical splice site/missense variants (N)*	10645	10521
Variants after filtering (N)&	485	327
Compound heterozygous variants (N)	12	3
Genes with compound heterozygous variants	<i>URB2, ARHGAP25, ZAR1, KIAA1211, VCAN, FER1L6, TNC, ANKRD26, MASTL, OR51G2, ZKSCAN2, CRISPLD2</i>	<i>SYNE2, SDK2, C18orf63</i>
Homozygous variants (N)	9	6
Genes with homozygous variants	<i>SPARC, SLC36A2, AHI1, C9orf131, EFHC2, USP27X, GPC4, ZNF717, KRT10</i>	<i>SPARC, DYSF, FAM114A2, TAGAP, C6orf118, ATAD3A</i>

* only variants covered by at least 5 reads and quality more than 20 were considered

& after exclusion of variants with (1) an allele frequency >5% in the 1000 genomes database or EVS; or (2) seen >30 samples in our in-house exome database or (3) seen as homozygote in the ExAC database